WARSAW UNIVERSITY OF TECHNOLOGY Index 351733
FACULTY OF CIVIL ENGINEERING
COMMITTEE FOR CIVIL AND WATER ENGINEERING
POLISH ACADEMY OF SCIENCES ISSN 1230-2945

DOI: 10.24425/ace.2022.140159

ARCHIVES OF CIVIL ENGINEERING

Vol. LXVIII ISSUE 1 2022

pp. 111–128

Research paper

Analysis of uniaxial compression of rock mass with parallel cracks based on experimental study and PFC^{2D} numerical simulation

Jie Yang[1], Haijun Chen[2], Xiong Liangxiao[3,4], Zhongyuan Xu[5], Tao Zhou[6], Changheng Yang[7]

Abstract: In this study, the uniaxial compression test and the numerical simulation of the two-dimensional particle flow code (PFC^{2D}) were used to study the mechanical properties and failure laws of rock masses with parallel cracks. The experiment considers the influences of crack length (l), crack angle (β_1, β_2), and numerical changes in the rock bridge length (h) and bridge angle (α) on failures of rock-like specimens. The results indicate that the uniaxial compressive strength (UCS) of the rock-like specimens with parallel cracks decreases with increasing l under different α values. The smaller angle between the preset crack and the loadinging direction (β) resulting in higher UCS. In addition, a larger h results in higher UCS in the specimen. When β_1 or β_2 is fixed, the UCS and elastic modulus of the specimen show an 'M' shape with an increase in α. Moreover, the crack growth or failure mode of samples with different l values is similar. When β_1 or β_2 is small, the failure of the specimen is affected by the development and expansion of wing cracks. If one of β_1 and β_2 is large, the failure of the specimen is dominated by the expansion and development of the secondary cracks which is generated at the tip of the prefabricated crack. Furthermore, when the angle between the prefabricated crack and the loading direction is $\beta_1 = 0°$, the rock bridge is less likely to reach penetration failure as h increases. Secondary crack connections between the prefabricated cracks occur only when α is small.

[1]Graduate student, College of Environment and Civil Engineering, Chengdu University of Technology, Chengdu, 610059, PR China, e-mail: yj1769151328@163.com, ORCID: 0000-0001-8430-480X

[2]Prof., PhD., Eng., Geotechnical Engineering Department, Nanjing Hydraulic Research Institute, Nanjing, Jiangsu Province, 210029, PR China, e-mail: hjchen@nhri.cn, ORCID: 0000-0003-0094-9649

[3]Associate Prof., PhD., Eng., School of Civil Engineering and Architecture, East China Jiaotong University, Nanchang 330013, PR China, e-mail: xionglx1982@126.com, ORCID: 0000-0002-6366-5187

[4]Associate Prof., PhD., Eng., Hunan Provincial Key Laboratory of Hydropower Development Key Technology, HydroChina Zhongnan Engineering Corporation, Changsha 410014, PR China, e-mail: xionglx1982@126.com, ORCID: 0000-0002-6366-5187

[5]PhD., Department of Earth Sciences, University of Delaware, Delaware 19716, United States, e-mail: zyxu@udel.edu, ORCID: 0000-0003-4303-1870

[6]Graduate student, College of Environment and Civil Engineering, Chengdu University of Technology, Chengdu, 610059, PR China, e-mail: 1312186954@qq.com

[7]Graduate student, School of Civil Engineering and Architecture, East China Jiaotong University, Nanchang 330013, PR China, e-mail: 771644322@qq.com ORCID: 0000-0001-8811-4632

When $\alpha > 30°$, the failure mode of the specimen is crack tip cracking which leads to penetration failure of the specimen, or the overall splitting failure.

Keywords: uniaxial compression, parallel cracks, numerical simulation, mechanical properties, failure characteristics

1. Introduction

Cracks are very common in rock masses and are important factors affecting rock mechanical properties. The geometric parameters and geometric distribution of cracks can directly reflect the rock's mechanical parameters such as uniaxial compressive strength (UCS) and elastic modulus. Parallel cracks are widely distributed in layered rock masses and are common phenomena in tunnel engineering and slope engineering practices.

Many aspects of rock crack research have been analyzed in experiments and numerical simulations. Yuan et al. [1] conducted uniaxial compression tests on red sandstone containing prefabricated cracks and analyzed the effects of crack inclination on the mechanical properties, crack propagation, and failure modes of the rock. The peak strength, maximum strain, and elastic modulus of the pre-cracked red sandstone increased with an increase in the crack inclination. Wen et al. [2] studied the mechanical behavior of pre-existing transverse cracks in lignite under uniaxial compression. Their results demonstrated that the pre-existing crack angle (β) changes the shape of the stress–strain curves and presented a series of unlimited compressive strength and crack initiation strength. Zhu et al. [3] analyzed the crack growth characteristics of double closed cracks in rock samples under uniaxial compression and studied the strength characteristics, crack growth, and coalescence laws of the different samples. Xiong et al. [4] studied the mechanical properties of artificial rocks with cross defects under uniaxial compression. Han et al. [5] studied the fracture evolution and failure mechanism of rock samples with cross defects under shear force and identified stages of linear elasticity, crack strengthening, plastic softening, and residual strength in the shearing process of rock-like materials with cross defects. Zhao et al. [6] conducted experimental and numerical studies on brittle rock samples containing internal cracks and cavities under uniaxial compression. The results showed that the shape and location of the internal defects and the volume of the internal open fracture had significant effects on the physical properties and spatial distribution of the specimen's shear and tensile failure. Feng et al. [7] studied the influence of two non-parallel fractures on the mechanical properties of rock samples under uniaxial compression. They showed that the strength, deformation characteristics, and coalescence mode of cracks are highly dependent on the geometric configuration of the cracks, the angle of fracture inclination ($a2$), the length of the rock bridge (d) and the angle of rock bridge (β). Afolagboye et al. [8] utilized a high-speed camera to study the cracking behavior and coalescence process of brittle materials with two non-parallel overlapping defects. The research results demonstrated that the geometry of the pre-existing defects would affect the crack initiation and coalescence behavior. Dey et al. [9] proposed that stress inhomogeneity under uniaxial or triaxial loading may induce the propagation of expansion cracks. They establish a theoretical model to predict the axial split of rock under uniaxial compression. Park et al. [10] conducted a study on the

crack initiation, propagation and merging of friction cracks in uniaxial compression. The results showed that there is almost no difference in the fracturing process between the open cracks and closed ones. Besides, their findings also demonstrated that the friction along the crack would increase the initial stress and coalescence. Stress and facilitate the view of connection through shear cracks.

Numerical methods were widely used in studying rock failure, especially Particle Flow Code (PFC). Chen et al. [11] used the two-dimensional PFC^{2D} program to study the strength and failure characteristics of rock samples containing different pore defects. They showed that the hole defects reduced the UCS, peak strain, and elastic modulus of the rock mass, accelerated the generation of cracks, and promoted the destruction of the rock. Shen et al. [12] calibrated a synthetic rock model according to an experimental resultusing PFC^{2D} based on sandstone characteristics. They studied the effect of defect width on the cracking behavior of a single-defect rock sample under uniaxial compression. Fakhimi et al. [13] adopted the discrete element method to perform a numerical analysis of the Pennsylvania blue sandstone, and proposed a size analysis method, which could simulate many deformation and failure characteristics of sandstone in conventional and some unconventional stress paths. Zeng et al. [14] used PFC^{2D} to study the mechanical properties and cracking behavior of specimens containing holes under uniaxial compression. They concluded that the shape of the hole has a considerable influence on the UCS and failure mode little influence on the elastic modulus. Wu et al. [15] used uniaxial compression testing combined with PFC^{2D} to study the effect of different horizontal distances (L or L') between the centroids of holes and cracks on the mechanical properties of pre-damaged rock-like materials. Haeri et al. [16] used PFC to study the influence of bedding on the failure mechanism of rock in a direct shear test. Zhao et al. [17] studied the failure mechanism of rock models with different fracture geometries under uniaxial compression. Bahaaddini et al. [18] used PFC^{3D} to investigate the effect of geometric parameters of joints on the rock mass failure mechanism, unconfined compressive strength and deformation modulus. It is found that the failure mode is determined principally by joint orientation and step angle and the joint orientation with respect to principal stress direction is the parameter with the greatest influence on rock mass properties. Wang et al. [19] used PFC^{2D} to simulate uniaxial compression in rhyolite with two coplanar fractures, and they analyzed influence of crack inclination (β), crack length (l), h, and crack width on the failure characteristics of cracked rock. Huang et al. [20] studied the cracking process of granite samples containing multiple pre-existing holes under uniaxial compression. They combined the results with three-dimensional PFC (PFC^{3D}) numerical analysis to determine that the failure mode of pre-drilled samples depends on the bridge angle (α) and the number of holes.

Experiment combined with numerical analysis is one of the main research methods at present. PFC is a relatively new method to study the crack propagation of rock-like materials as it is able to describe the characteristics of crack propagation from a microscopic perspective. Predecessors have done a lot of research on fractured rock masses, but there are few researchers focused on the mechanical properties and failure laws of fractured rock masses with different geometric configurations, especially parallel fractured rock masses. To address this lack of research, this paper aims to study the mechanical properties and fracture propagation of parallel fractured rock through experiments and PFC^{2D} simula-

tions. Our simulation materials are fabricate rock-like specimens with different values of l, β_1, β_2, h and α. Uniaxial compression testing and PFC^{2D} were used to study the mechanical properties and failure laws of rock masses with parallel fractures under uniaxial compression loadinging.

2. Experimental set-up

2.1. Sample preparation and the mark of the geometric position of the cracks

The present test used cement mortar as the rock simulation material. No. 32.5 cement was used in this test; the sand was intermediate standard sand; the specimen mold size was 100 mm × 100 mm × 100 mm, and the prefabricated cracks were formed by polyvinyl chloride (PVC) plates with a thickness of 1 mm. The specimen was composed of cement mortar with a water–cement ratio of 0.65. After the mortar was poured into the mold and was allowed to initially set, the PVC plate was inserted according to the positional relationship shown in Fig. 1. After the specimen cured in the mold for 24 h, the plate was removed to form a plane penetrating crack. The length of the crack is l, the length of the rock bridge is h, and the angle between the rock bridge and the horizontal direction is recorded as α. The angle between the crack and the vertical line of the end point of the rock bridge is β_1 upward, and β_2 downward. The test specimens were divided into type I parallel cracks (The crack angle is β_1) and type II (The crack angle is β_2) parallel cracks according to the position of the cracks.

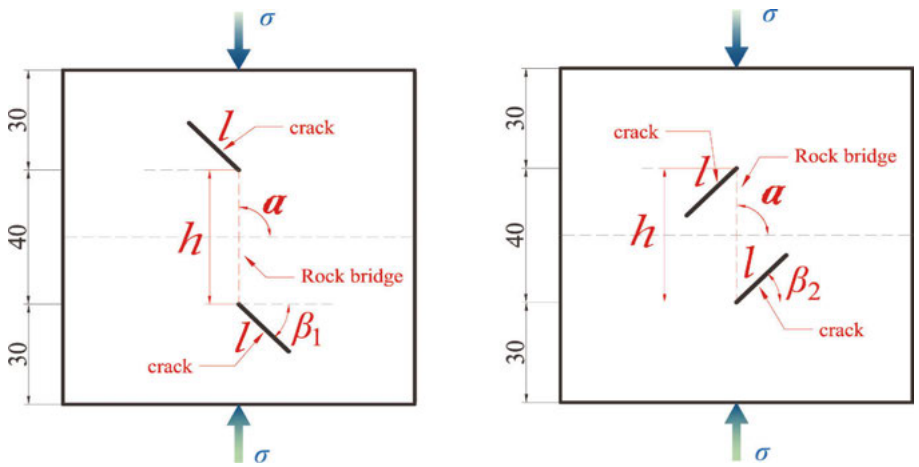

a) Type I parallel crack b) Type II parallel crack

Fig. 1. Geometric locations of the crack and the rock bridge. The length of the crack is l; the length of the rock bridge is h; the angle between the rock bridge and the horizontal direction is α; and the angle between the crack and the vertical line of the end point of the rock bridge is β_1 (upward) and β_2 (downward). (Unit: mm)

2.2. Test setup and simulated material data

The specimens were cured for 28 days and held for 7 days to perform the uniaxial compression test. During the experiment, the loadinging rate was set to 1 mm/min, and the testing machine collected data in 0.1 s increments. To reduce the error, three parallel test specimens were set for each group of tests, and the average compressive strength was calculated. In the test, three complete specimens were prepared without cracks, and then basic mechanical tests were conducted on them. The average values of the measured data, as given in Table 1, reflect good results for using rock simulation specimens to study the mechanical properties.

Table 1. Test material parameters

Density [g/cm^{-3}]	Compressive strength [MPa]	Elastic modulus [GPa]
2.25	25.85	1.72

2.3. Test grouping

The experimental groupings of type I (type II) parallel cracks of angle type β_1 (β_2) are shown in Table 2 (Table 3). In addition to the parameters shown in the tables, indoor tests included settings of l = 20 mm; h = 20 mm; β_1 = 120°, 135°, 150°, and 180°; and β_2 = 120°, 135°, and 150°

Table 2. Groups of Type I parallel crack experiment

β_1 (°)	α (°)	h (mm)	l (mm)
0	0, 30, 45, 60, 90	10, 20, 30, 40	10, 20, 30, 40
30	0, 30, 45, 60, 90	20	20
45	0, 30, 45, 60, 90	20	20
60	0, 30, 45, 60, 90	20	20
90	0, 30, 45, 60, 90	20	20

Table 3. Groups of Type II parallel crack experiment

β_2 (°)	α (°)	h (mm)	l (mm)
0	0, 30, 45, 60, 90	10, 20, 30, 40	10, 20, 30, 40
30	0, 30, 45, 60, 90	20	20
45	0, 30, 45, 60, 90	20	20
60	0, 30, 45, 60, 90	20	20
90	0, 30, 45, 60, 90	20	20

3. Analysis of test results

3.1. Analysis of crack length

To explore the influence of l, $h = 10$ and $\beta_1 = 0°$ were fixed. By adjusting α, the influence of l on the mechanical properties of the specimen was determined. In the experiment, α was set to 0°, 30°, 45°, 60°, and 0°, and l was set to 10 mm, 20 mm, 30 mm, and 40 mm. Fig. 2 shows that when $h = 10$ and $\beta_1 = 0°$, the change in the elastic modulus and compressive strength of the specimen decreased with an increase in l of the parallel cracks.

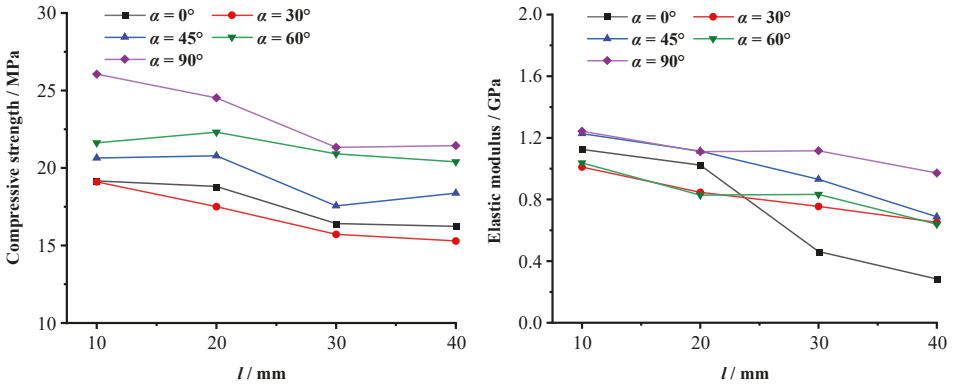

a) Compressive strength b) Elastic Modulus

Fig. 2. The effect of crack length on compressive strength and elastic modulus

3.2. Analysis of the crack angle

To determine the influence of β_1 and β_2 on the mechanical properties of the specimen under different values of α, l and h remained unchanged; specifically, l and h were both fixed at 20 mm, and the test was conducted by adjusting β_1, β_2, and α.

Figs. 3a and 3b show that when $\alpha = 0°$, the compressive strength of the two groups of test specimens is maximum when $\beta_1 = 90°$ and $\beta_2 = 90°$ and when $\beta_1 = 0°$and $\beta_2 = 0°$. When $\alpha = 90°$, the compressive strength of the two groups of test specimens is highest when $\beta_1 = 0°$ and $\beta_2 = 0°$ and lowest when $\beta_1 = 90°$ and $\beta_2 = 90°$. That is, when $\alpha = 0°$, as β_1 and β_2 increased, the included angle (β) between the crack and the direction of loading become smaller, and the compressive strength of the specimen increases. When $\alpha = 90°$, with an increase in β_1 and β_2, the included angle (β) with the loading direction increases, and the compressive strength of the specimen decrease. It can be concluded that the angle between the crack and the loading direction in the parallel crack specimen has a significant impact on the mechanical properties of the specimen, a larger angle (β) in the range of 0° to 90° results in lower peak compressive strength of the specimen.

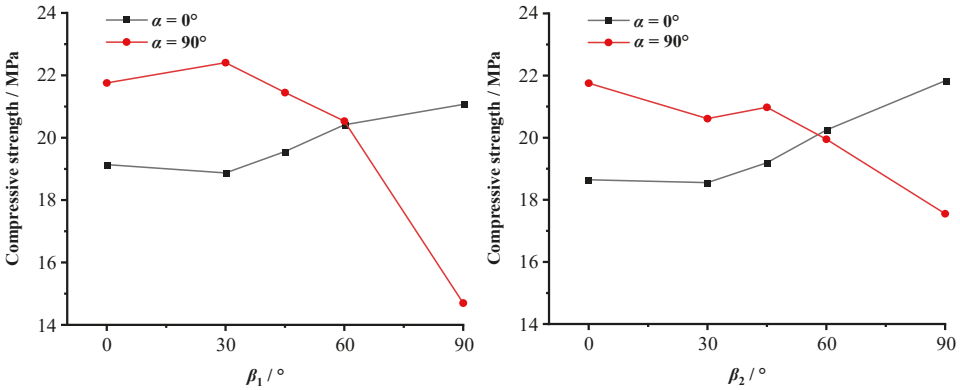

a) Type I crack $\alpha = 0°$ and 90° b) Type II crack $\alpha = 0°$ and 90°

Fig. 3. Relationship between crack angle and compressive strength

The changes in the elastic modulus of the two groups of tests are shown in Fig. 4a and 4b. It displays that the elastic modulus of the specimen increases with the increasing crack angles β_1 and β_2 when the rock bridge $\alpha = 0°$. In the case of $\alpha = 90°$, as the test setup crack angles β_1 and β_2 increase, the elastic modulus of the test piece decreases. The variation trend of elastic modulus is similar to that of compressive strength. In the range of 0° to 90°, the greater the angle β, the lower the elastic modulus of the specimen.

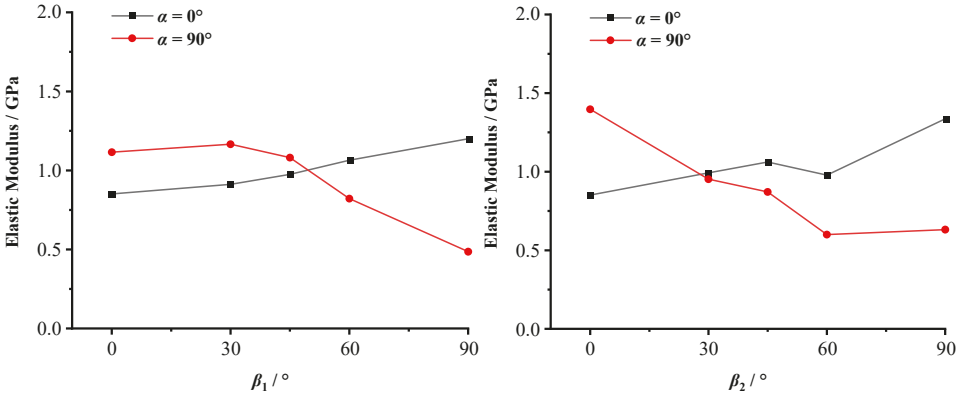

a) Type I crack $\alpha = 0°$ and 90° b) Type II crack $\alpha = 0°$ and 90°

Fig. 4. Relationship between crack angle and elastic modulus

The compressive strength comparison chart indicates that when $\alpha = 30°$, 45°, and 60°, the compressive strength of the specimen under other α values also show similar laws. At β_1 (type I parallel crack), the image shows a trend of first increase, then decrease, and then

increase again (Fig. 5a), whereas at β_2 (type II parallel crack), the change trend displays decrease-increase-decrease. When α is different, the image shifted slightly. However, the change in the compressive strength of the specimen is still related to the change in the angle between the crack and the loadinging direction, such as a smaller (larger) angle resulted in higher (lower) the compressive strength of the specimen. This result is consistent with the above conclusion.

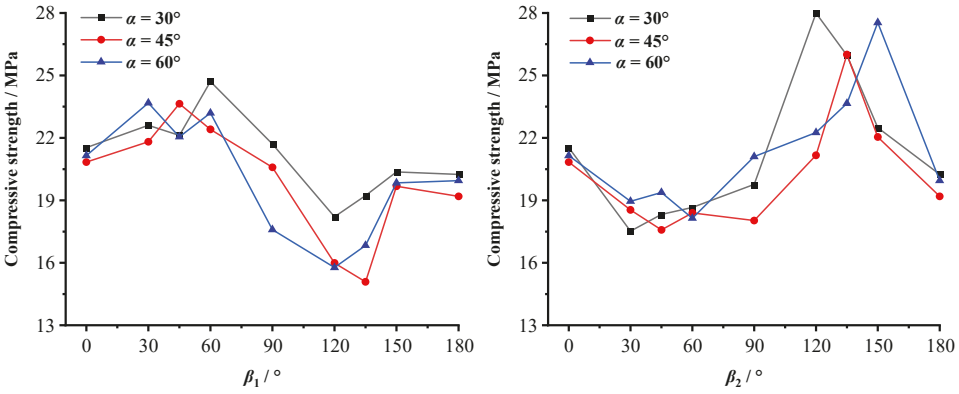

a) Type I crack when α = 0°, 30°, 90° b) Type II crack when α = 0°, 30°, 90°

Fig. 5. Comparison of experimental data with different fracture angles

3.3. Analysis of the length of the rock bridge

When analyzing the influence of the change in h on the mechanical properties of the test specimen, the angle between the set crack and the rock bridge was fixed (i.e., $\beta_1 = 0°$ remained unchanged), and two sets of comparative tests with l = 10 mm and 20 mm were used when α was set to 0°, 30°, 45°, 60°, and 90° and h was set to 10 mm, 20 mm, 30 mm, and 40 mm.

According to the test results in Fig. 6, the impact of the length of the rock bridge on the compressive strength of the specimen is obvious. When l and $\beta_1 = 0°$ are constant, the compressive strength and elastic modulus of the two experimental specimens with l = 10 mm and 20 mm under different α values increase with an increasing h.

The changes in the compressive strength and elastic modulus of the specimens are similar and are greatly associated with the geometry of cracks. The compressive strength and elastic modulus of the sample decrease with the increasing crack length and with the increasing angle between crack and loadinging direction, which are similar to the conclusions made by Yuan [1] and Feng [7]. In order to further study the influence of the geometric position of rock bridge and cracks on the compressive strength and elastic modulus, we also took into account the length and angle of rock bridge and the angle of cracks.

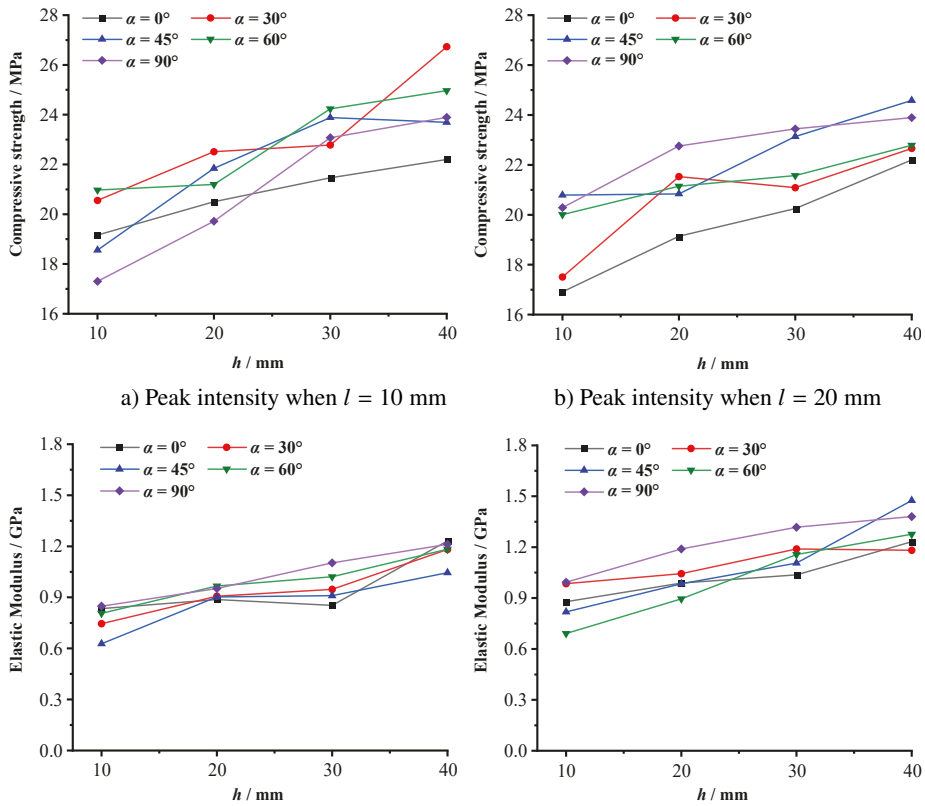

a) Peak intensity when l = 10 mm

b) Peak intensity when l = 20 mm

c) Elastic modulus when l = 10 mm

d) Elastic modulus when l = 20 mm

Fig. 6. Comparison of test data for changes in h

3.4. Analysis of rock bridge angle

During the test design, l = 20 mm and h = 20 mm were fixed, and the influence of the geometric position of the rock bridge under different parallel crack angles on the compressive strength and elastic modulus of the specimen was studied. In this group of experiments, the values of α, β_1, and β_2 were all 0°, 30°, 45°, 60°, and 90°.

Fig. 7a and 7b shows that when l = 20 mm, h = 20 mm, and the angle between the crack and the rock bridge was fixed (i.e., when the value of β_1 or β_2 is fixed), the test curves of β_1 = 90° and β_2 = 90° essentially show a downward trend. When β_1 = 90°, the two cracks are coplanar; when β_2 = 90°, the positions of the two prefabricated cracks coincide with each other. The relationship between the compressive strength of the specimen and the angle of the crack in these two cases are essentially the same as the previous conclusion, which is a smaller the angle between the crack and the loadinging direction results in higher compressive strength. Therefore, as α increases, the angle between the crack and the loadinging direction is greater, and the compressive strength of the specimen shows a downward trend. With other values of β_1 and β_2, the trend of the compressive strength of

the specimen and the angle of the rock bridge display an M-shaped. When $\alpha = 30°$ and 60°, the compressive strength of the specimen larger, and that of other α values is less than the specimens under $\alpha = 30°$ and 60°. With different values of β_1 and β_2, the curves of the elastic modulus of the test piece with the angle of the rock bridge are shown in Fig. 7c and 7d. From the image, except for $\beta_1 = 90°$ and $\beta_2 = 90°$, the curves also present an M-shape. The curves of $\beta_1 = 90°$ and $\beta_2 = 90°$ also show a downward trend with an increase in α.

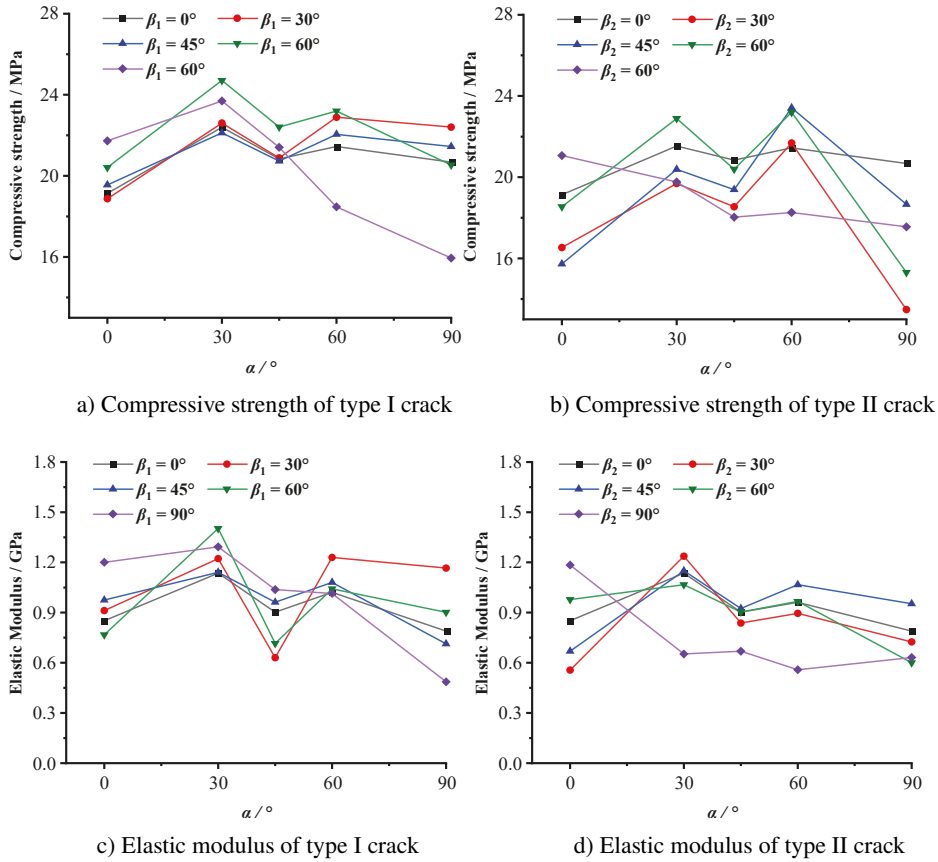

a) Compressive strength of type I crack

b) Compressive strength of type II crack

c) Elastic modulus of type I crack

d) Elastic modulus of type II crack

Fig. 7. Test of angle change of cracks and rock bridges

4. Numerical simulation analysis

4.1. Numerical model and parameter sittings

The numerical simulation adopted PFC^{2D} and established a calculation model through the parallel bonding method. The PFC^{2D} model is shown in Fig. 8. The calibration of the

calculated parameters was based on the test data of the simulated material, and a set of particle flow simulation parameters were obtained after repeated trial calculations. The simulation parameter settings are shown in Table 4.

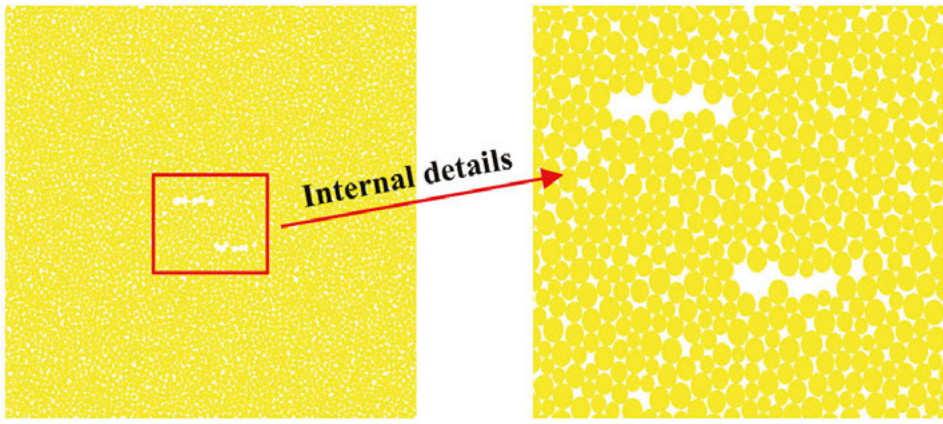

a) Complete schematic b) Detailed schematic

Fig. 8. Schematic diagram of PFC^{2D} model

Table 4. Calculation parameters of simulated rock materials

Effective modulus (GPa)	Minimum particle radius (mm)	Maximum particle radius (mm)	Density (g/cm^{-3})	Stiffness ratio	Coefficient of friction
1.4	1.0	1.66	1.96	1.0	0.5

4.2. Numerical model verification

According to the numerical simulation results in Fig. 9, the h was fixed at 10 mm, and the compressive strength and elastic modulus of the specimen at any α value decrease with an increase in the preset parallel l. This result is consistent with the conclusion drawn in Section 3.1.

At l = 20 mm and h = 20 mm, at different α values, the angle between the crack and the rock bridge was fixed in the PFC^{2D} simulation. The results of β_1 at 0°, 30°, 45°, 60°, and 90° are shown in Fig. 10b. When the angle between the rock bridge and the crack was fixed, under different rock bridge angles and crack angles, the simulated test peak strength curve essentially showes an M-shape, which is equivalent to the indoor test result given in Fig. 10a.

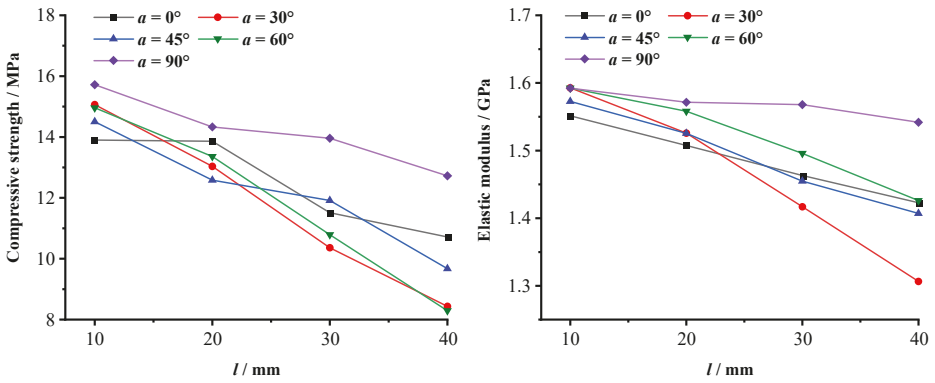

a) Compressive strength under different values of l b) Elastic modulus under different values of l

Fig. 9. Simulation results for l

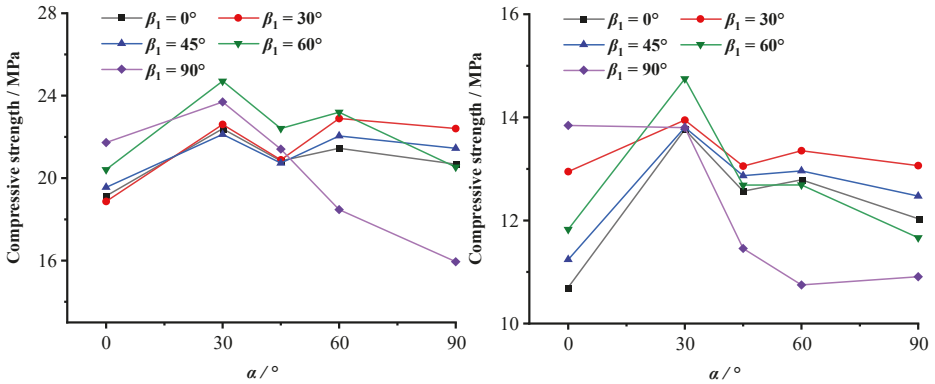

a) Test results b) Simulation results

Fig. 10. Simulation verification of α test

4.3. Analysis of crack propagation

In the failure diagrams of specimens with different length cracks, the failure modes of the specimens are similar under different prefabricated crack lengths. The main reason is development and expansion of the same type of cracks lead to failure in the specimens. However, as the length of the preset cracks increases, the number of cracks generated during compression also increases. We compared the PFC^{2D} simulated diagram and the experimental rupture diagram with l values equal 10 mm, 20 mm, 30 mm, and 40 mm at $\alpha = 0$. The development of wing cracks on both sides of the prefabricated cracks is the major cause of damage in the specimens, as shown in Fig. 11. As the length of the preset crack increases, the number of wing cracks generated on both sides of the crack in compression also increase. In the PFC^{2D} simulated diagrams and destruction diagrams of l = 10 mm and l = 20 mm, distal cracks are developed. When the length of the horizontal crack increases, the number of distal crack development is reduce.

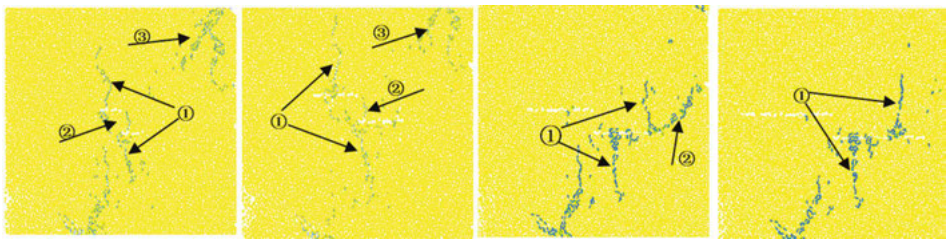

a) l = 10 mm b) l = 20 mm c) l = 30 mm d) l = 40 mm

a) l = 10 mm b) l = 20 mm c) l = 30 mm d) l = 40 mm

Fig. 11. Crack rupture diagram of different lengths. Circled numbers 1–4 indicate the wing cracks developed on the side of the preset crack, secondary cracks generated at the tips of the cracks, and cracks developed at the distal end of the specimen, splitting crack, respectively

Under different crack angles, the failure modes of the specimens are significantly different, as shown in Fig. 12. When the crack angle is small, wing cracks would develop at the ends and sides of the preset cracks, and their propagation direction is approximately along the loading direction. This is consistent with the viewpoint proposed by Sagong [21] that the wing crack develops at a certain angle to the crack and expands stably in the direction of maximum compression. The failure of the specimen is caused by a penetrated crack that is formed by the lap joint between the wing crack and the prefabricated one, and this failure belongs to the type of axial compression failure. Zhao [22] proposed that in the failure characteristics of single-crack rock materials, the location of the maximum principal strain concentration would change from the inside of a crack to the tip of it with the increasing inclination angle. In this study, in the experiments and simulation diagrams with the increase of the inclination angle, the more number of micro-fractures produced at the tip of the fracture, the more complicated the mechanics of the tip of the fracture. With the increase of the inclination angle, the stress concentration shifts to the tip of the prefabricated crack. From the experimental perspective, it is demonstrated that the number of wing cracks produced in the middle of the prefabricated cracks would decrease with the increase of the crack angle, while the number of secondary cracks produced at the tip of the cracks would increase with the increase of the crack angle. Conclusion can be drawn that with an increase in the crack angle, the number of wing cracks decrease, the number of secondary cracks increase, and the fracture of the specimen changed from axial compression to tension–shear mixed fracture.

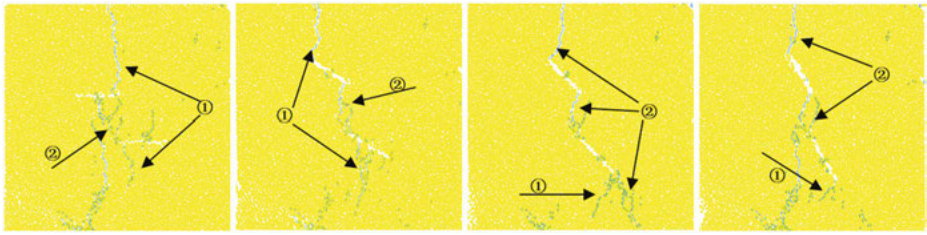

a) $\beta_1 = 0°$ b) $\beta_1 = 30°$ c) $\beta_1 = 45°$ d) $\beta_1 = 60°$

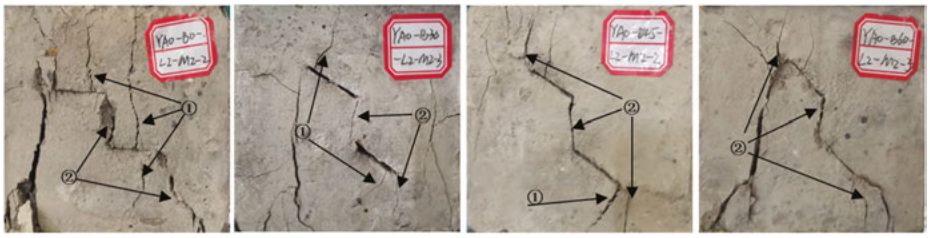

a) $\beta_1 = 0°$ b) $\beta_1 = 30°$ c) $\beta_1 = 45°$ d) $\beta_1 = 60°$

e) $\beta_1 = 90°$ e) $\beta_1 = 90°$

Fig. 12. Crack expansion diagram with different crack angles

In the case of $\alpha = 0$ and $l = 20$ mm, we compared the four groups of test and simulation results with h values of 10 mm, 20 mm, 30 mm, and 40 mm. The results of Fig. 13 show that the fracture failure of specimens with different h values is mainly caused by the development and expansion of wing cracks. When the h is small, secondary cracks appear between the prefabricated cracks, which facilitated breakage in the rock bridge results in a breakage through the entire specimen. As h increases, the number of secondary cracks initiate between the prefabricated cracks decreases, and the probability of rock bridge penetration and failure decrease. The simulation diagram indicates that the damage of the specimen is mainly penetration damage caused by expansion of the wing cracks or the overall damage of the specimen.

The failure and simulation diagrams of the test specimens under different α values when $l = 20$ mm, $h = 20$ mm, and $\beta_1 = 0°$ show the results in Fig. 14. The rock bridge penetration failure occurs only in the test of $\alpha = 0°$ and $\alpha = 30°$. In these two groups of experiments, the development of internal wing cracks and secondary oblique cracks lead

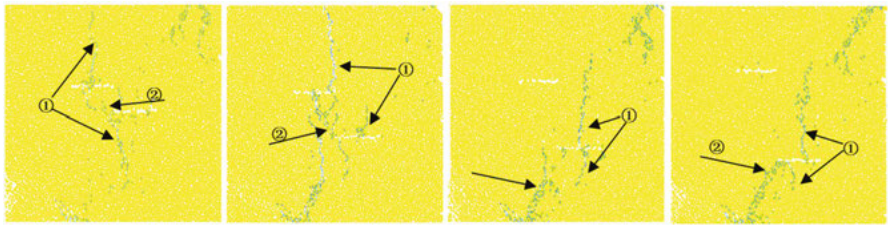

a) l = 10 mm b) l = 20 mm c) l = 30 mm d) l = 40 mm

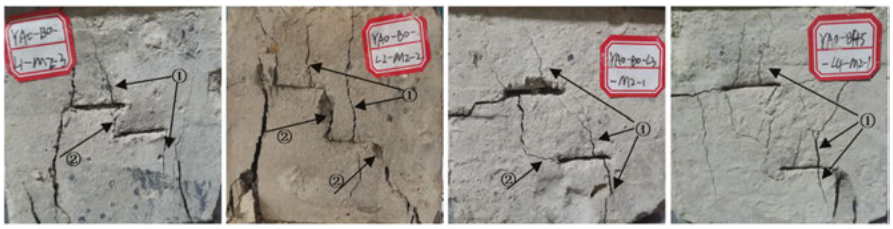

a) l = 10 mm b) l = 20 mm c) l = 30 mm d) l = 40 mm

Fig. 13. Fracture diagram of specimens with different h values

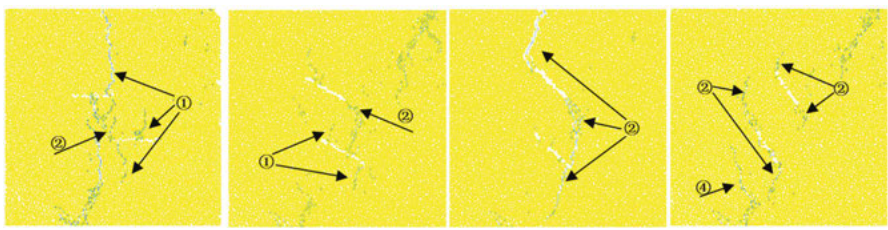

a) β_1 = 0° b) β_1 = 30° c) β_1 = 45° d) β_1 = 60°

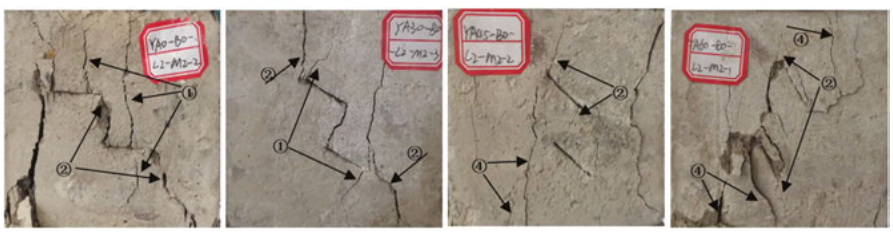

a) β_1 = 0° b) β_1 = 30° c) β_1 = 45° d) β_1 = 60°

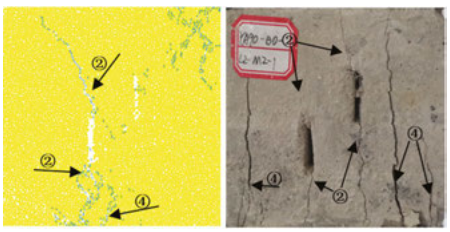

e) β_1 = 90° e) β_1 = 90°

Fig. 14. Cracking diagram of specimens with different α values

to penetration failure or overall failure of the specimens. In the test group of $\alpha > 30°$, the development of secondary cracks generated at both ends of the prefabricated cracks leads to penetration failure of the specimens as the main failure mode. The destruction diagram of the test at $\alpha > 30°$ shows that the number of split cracks increases, and the simulation diagram appears only at 60° and 90°, indicating that at $l = 20$ mm, $h = 20$ mm, $\beta_1 = 0°$ and $\alpha > 30°$, the specimen is more prone to splitting failure.

5. Conclusions

1. The compressive strength and elastic modulus of the rock-like specimens with parallel cracks under different α values decrease with an increase in the preset l. In addition, the smaller included angle β between the preset crack and the loading direction in the range of 0°–90°, the higher the compressive strength and elastic modulus of the specimen.
2. A greater h value leads to a higher compressive strength of the specimen. When the angle between the crack and the rock bridge (β_1 and β_2) is fixed, an increase in α causes the change of the compressive strength and elastic modulus of the specimen to assume M-type.
3. When $\alpha = 0°$ and $\beta_1 = 0$, the failure modes of the specimens with different preset l were similar, but as l increases, the number of wing cracks initiate on both sides of the crack increases. When the prefabricated β_1 is small, the damage to the specimen is affected by the development of wing cracks, and the damage is caused mainly by axial pressure. When the prefabricated β_1 is large, the failure of the specimen is dominated by the development of the secondary crack initiated at the tip of the prefabricated crack, and the specimen experience a mixed effect of tensile and shear failure.
4. When the angle between the prefabricated crack and the loading is 0°, as the h increases, the rock bridge is less likely to undergo penetration failure. Only when α is small, the prefabricated cracks overlapped with the secondary cracks. When the α is greater than 30°, the failure mode of the specimen is crack tip cracking which leads to penetration failure of the specimen, or the overall splitting failure.

References

[1] Y. Yuan, J. Fu, X. Wang, X. Shang, "Experimental Study on Mechanical Properties of Prefabricated Single-Cracked Red Sandstone under Uniaxial Compression", *Advances in Civil Engineering*, 2020, vol. 2020, DOI: 10.1155/2020/8845368.

[2] J.H. Wen, T. Zhan, D. Ashley.P, T. Ali, "The mechanical behaviour of pre-existing transverse cracks in lignite under uniaxial compression", *Geomechanics and Geophysics Geo-Energy and Geo-Resources*, 2021, vol. 7, DOI: 10.1007/s40948-020-00201-w.

[3] J.M. Zhu, H.L. Yu, "Analysis of Crack Propagation Characteristics of Rock-like Material with Double Closed Cracks Under Uniaxial Compression", *Geotechnical and Geological Engineering*, 2020, vol. 38, pp. 6499–6509, DOI: 10.1007/s10706-020-01451-x.

[4] L.X. Xiong, H.J. Chen, D.X. Geng, "Uniaxial Compression Study on Mechanical Properties of Artificial Rock Specimens with Cross-Flaws", *Geotechnical and Geological Engineering*, 2021, vol. 39, pp. 1667–1681, DOI: 10.1007/s10706-020-01584-z.

[5] W. Han, Y.J. Jiang, H.J. Luan, J.K. Liu, X.L. Wu, Y.T. Du, "Fracture evolution and failure mechanism of rock-like materials containing cross-flaws under the shearing effect", *Theoretical and Applied Fracture Mechanics*, 2020, vol. 110, DOI: 10.1016/j.tafmec.2020.102815.

[6] Y.S. Zhao, Y.T. Gao, S.C. Wu, "Experimental and Numerical Studies of Brittle Rock-Like Samples with Internal Open Fractures and Cavities Under Uniaxial Compression", *Arabian Journal for Science and Engineering,* 2020, vol. 45, pp. 8349–8368, DOI: 10.1007/s13369-020-04712-2.

[7] P. Feng, F. Dai, Y. Liu, N. Xu, T. Zhao, "Influence of two unparallel cracks on the mechanical behaviours of rock-like specimens subjected to uniaxial compression", *European Journal of Environmental and Civil Engineering,* 2020, vol. 24, pp.1643-1663, DOI: 10.1080/19648189.2018.1481770.

[8] L.O.Afolagboye, J. He, S. Wang, "Experimental study on cracking behaviour of moulded gypsum containing two non-parallel overlapping flaws under uniaxial compression", *Acta Mechanica Sinica*, 2017, vol. 33, pp. 394–405, DOI: 10.1007/s10409-016-0624-9.

[9] T.N. Dey, C.Y. Wang, "Some mechanisms of microcrack growth and interaction in compressive rock failure", *International Journal of Rock Mechanics and Mining Sciences & Geomechanics Abstracts,* 1981, vol. 18, pp. 199–209, DOI: 10.1016/0148-9062(81)90974-8.

[10] C.H. Park, A. Bobet, "Crack initiation, propagation and coalescence from frictional flaws in uniaxial compression", *Engineering Fracture Mechanics*, 2010, vol. 77, pp. 2727–2748, DOI: 10.1016/j.engfracmech.2010.06.027.

[11] S.J. Chen, Z.G. Xia, F. Feng, D.W. Yin, "Numerical study on strength and failure characteristics of rock samples with different hole defects", *Bulletin of Engineering Geology and the Environment*, 2021, vol. 80, pp. 1523–1540, DOI: 10.1007/s10064-020-01964-y.

[12] J.Y. Shen, S.X. Zhan, M. Karakus, J.P. Zuo, "Effects of flaw width on cracking behavior of single-flawed rock specimens", *Bulletin of Engineering Geology and the Environment*, 2021, vol. 80, pp. 1701–1711, DOI: 10.1007/s10064-020-02029-w.

[13] A. Fakhimi, T. Villegas, "Application of Dimensional Analysis in Calibration of a Discrete Element Model for Rock Deformation and Fracture", *Rock Mechanics and Rock Engineering*, 2007, vol. 40, pp. 193–211, DOI: 10.1007/s00603-006-0095-6.

[14] W. Zeng, S.Q. Yang, W.L. Tian, "Experimental and numerical investigation of brittle sandstone specimens containing different shapes of holes under uniaxial compression", *Engineering Fracture Mechanics*, 2018, vol. 200, pp. 430–450, DOI: 10.1016/j.engfracmech.2018.08.016.

[15] T. Wu, Y. Gao,Y. Zhou, J. Li, "Experimental and numerical study on the interaction between holes and cracks in rock-like materials under uniaxial compression", *Theoretical and Applied Fracture Mechanics*, 2020, vol. 106, DOI: 10.1016/j.tafmec.2020.102488.

[16] H. Haeri, V. Sarfarazi, Z.M. Zhu, H.R. Nejati, "Numerical simulations of fracture shear test in anisotropy rocks with bedding layers", *Advances in Concrete Construction*, 2019, vol. 7, no. 4, pp. 241–247, DOI: 10.12989/acc.2019.7.4.241.

[17] T.B. Zhao, W.Y. Guo, Y.L. Tan, F.H. Yu, B. Huang, L.S. Zhang, "Failure mechanism of layer-crack rock models with different vertical crack geometric configurations under uniaxial compression", *Advances in Mechanical Engineering*, vol. 9, no. 11, DOI: 10.1177/1687814017737259.

[18] M. Bahaaddini, G. Sharrock, B.K. Hebblewhite, "Numerical investigation of the effect of joint geometrical parameters on the mechanical properties of a non-persistent jointed rock mass under uniaxial compression", *Computers and Geotechnics*, 2013, vol. 49, pp. 206–225, DOI: 10.1016/j.compgeo.2012.10.012.

[19] Z.C. Wang, W.T. Zhao, K. Pan, "Analysis of fracture evolution characteristics of coplanar double fracture rock under uniaxial compression", *Geotechnical and Geological Engineering*, 2020, vol. *38, pp.* 343–352, DOI: 10.1007/s10706-019-01022-9.

[20] Y.H. Huang, S.Q. Yang, W.L. Tian, "Cracking process of a granite specimen that contains multiple pre-existing holes under uniaxial compression", *Fatigue and Fracture of Engineering Materials and Structures*, 2019, vol. 42, pp. 1341–1356, DOI: 10.1111/ffe.12990.

[21] M. Sagong, A. Bobet, "Coalescence of multiple flaws in a rock-model material in uniaxial compression", *International Journal of Rock Mechanics and Mining Sciences,* 2002, vol. 39, no. 2, pp. 229–241, DOI: 10.1016/S1365-1609(02)00027-8.

[22] C. Zhao, J.L. Niu, Q.Z. Zhang, C.F. Zhao, Y.M. Zhou, "Failure characteristics of rock-like materials with single flaws under uniaxial compression", *Bulletin of Engineering Geology and the Environment*, 2019, vol. 78, pp. 593–603, DOI: 10.1007/s10064-018-1379-2.

Received: 30.03.2021, Revised: 27.07.2021